Bottom-quark fragmentation: comparing results from tuned event generators and resummed calculations

G. Corcella[1] and V. Drollinger[2]

[1]*Department of Physics, CERN*
Theory Division
CH-1211 Geneva 23, Switzerland

[2]*Dipartimento di Fisica Galileo Galilei, Università di Padova*
and INFN, Sezione di Padova
Via Marzolo 8, I-35131 Padova, Italy

Abstract

We study bottom-quark fragmentation in e^+e^- annihilation, top and Higgs decay $H \to b\bar{b}$, using Monte Carlo event generators, as well as calculations, based on the formalism of perturbative fragmentation functions, which resum soft- and collinear-radiation effects in the next-to-leading logarithmic approximation. We consider the PYTHIA and HERWIG generators, and implement matrix-element corrections to the parton shower simulation of the $H \to b\bar{b}$ process in HERWIG. We tune the Kartvelishvili, string and cluster models to B-hadron data from LEP and SLD, and present results in both x_B and moment spaces. The B-hadron spectra yielded by HERWIG, PYTHIA and resummed calculations show small discrepancies, which are due to the different approaches and models employed and to the quality of the fits to the e^+e^- data.

1 Introduction

Heavy-flavour phenomenology is currently one of the most lively fields of investigation, in both experimental and theoretical particle physics. In this paper, we consider B-hadron production in e^+e^- annihilation ($e^+e^- \to b\bar{b}$), top decay ($t \to bW$) and the decay of the Standard Model Higgs boson $H \to b\bar{b}$. In fact, data on b-flavoured hadron production from SLD [1] and LEP [2,3] experiments have been available for a few years, and they can be used to predict b-quark fragmentation in other processes. Bottom fragmentation in top decay is indeed one of the main sources of uncertainties on the top-mass reconstruction at the Tevatron [4] and the LHC. In particular, the analysis in Ref. [5], where the top-quark mass is determined from the invariant mass of three leptons (one lepton from the W decay and two leptons from a $J/\psi \to \ell^+\ell^-$ decay), depends on a proper description of the fragmentation of b quarks into B hadrons which decay further to J/ψ's. As for $H \to b\bar{b}$, the detection of this process is impossible in the channel $gg(q\bar{q}) \to H \to b\bar{b}$ at hadron colliders, because of the large irreducible $b\bar{b}$ background. The solution to this problem is to look for $H \to b\bar{b}$ in associated production channels. The most relevant search channels are Higgs production in association with a vector boson at the Tevatron [6], and in association with a W boson [7] or with $t\bar{t}$ pairs [8] at the LHC. In such channels, the $H \to b\bar{b}$ decay mode can be probed for a Higgs mass up to $m_H \lesssim 135$ GeV. For heavier Higgs bosons, the decay to $b\bar{b}$ might be accessible in Two-Higgs Doublet Models, with enhanced Higgs couplings to bottom quarks [9]. In all cases, a good understanding of bottom fragmentation in Higgs decays is important for the Higgs mass reconstruction and the identification of b-jets, which both depend on the properties of the Higgs decay products.

In order to perform accurate searches and measurements, the use of precise QCD calculations will be fundamental. In particular, fixed-order calculations are reliable enough to predict total cross sections or widths, but differential distributions exhibit terms, corresponding to collinear or soft parton radiation, that need to be summed to all orders to obtain a meaningful result. An example is the large term $\sim \alpha_S \ln(Q^2/m^2)$, where Q is the hard scale of the process and m the heavy-quark mass, which appears in the energy distribution of a heavy quark at next-to-leading order (NLO).

A possible approach to study b-quark production in the considered processes is based on the perturbative fragmentation formalism [10]. The NLO heavy-quark energy spectrum is expressed as the convolution of a coefficient function, describing the emission of a massless parton, and a perturbative fragmentation function $D(m_b, \mu_F)$, associated with the transition of a massless parton into a massive quark. The dependence of $D(m_b, \mu_F)$ on the factorization scale μ_F is determined by using the Dokshitzer–Gribov–Lipatov–Altarelli–Parisi (DGLAP) evolution equations [11, 12], once an initial condition at a scale μ_{0F} is given. The initial condition of the perturbative fragmentation function, first computed in [10], has been proved to be process-independent in [13]. Solving the

DGLAP evolution equations we can resum the large $\ln(Q^2/m^2)$ (collinear resummation).

Moreover, heavy-quark energy distributions present terms that are enhanced when the energy fraction x approaches 1. Such contributions can be resummed following the general method of [14,15] (soft or threshold resummation). Soft and collinear resummations in the next-to-leading logarithmic approximation (NLL) have been implemented for b production in e^+e^- annihilation [10,13], top-quark [16,17] and Higgs [18] decays, in the framework of perturbative fragmentation functions.

An alternative approach to address heavy-quark production and resum terms corresponding to soft and colliner radiation consists in using Monte Carlo event generators. Standard Monte Carlo programs, such as HERWIG [19] or PYTHIA [20,21], simulate multiple emissions in the soft or collinear approximation, and are provided with matrix-element corrections [22,23] to describe hard or large-angle radiation.

In order to describe hadronic spectra, perturbative calculations and Monte Carlo parton showers need to be supplemented by models describing the hadronization. Calculations based on the fragmentation-function approach typically predict hadron-level energy distributions convoluting the partonic spectra with a non-perturbative fragmentation function, such as the Kartvelishvili [24] or the Peterson [25] models. These models contain parameters that need to be fitted to experimental data. More recently [26], it was suggested that one can fit directly the N-moments of heavy-hadron cross sections and extract the moments of the non-perturbative fragmentation function, with no need to assume any functional form in x-space. Likewise, Monte Carlo event generators simulate the hadronization using appropriate non-perturbative models, such as the cluster model [27] and the string model [28], for HERWIG and PYTHIA, respectively.

The outline of this paper is the following. In section 2 we review collinear and soft resummations in the framework of perturbative fragmentation functions. In section 3 we discuss Monte Carlo parton shower algorithms. Section 4 describes matrix-element corrections to parton-shower simulation and, in particular, the implementation of such corrections to $H \to b\bar{b}$ processes in HERWIG. In sections 5 and 6 we shall present our results on B-hadron production in e^+e^- annihilation, top and Higgs decays, in x and moment space respectively, after tuning the hadronization models to e^+e^- data from LEP and SLD. Section 7 summarizes the main results and gives some concluding remarks.

2 Perturbative fragmentation functions

In this section we shall review the main points of the perturbative fragmentation approach and of the implementation of collinear and soft resummations. We shall consider

b production at next-to-leading order in Z, top or Higgs decays, i.e.

$$P(Q) \to b(p_b)\bar{b}(p_{\bar{b}})\,(g(p_g))\,, \tag{1}$$

with $P = Z$ or H, and

$$t(Q) \to b(p_b)W(p_W)\,(g(p_g))\,. \tag{2}$$

The energy spectrum of a massive b quark is given by the following general result:

$$\frac{1}{\Gamma_0}\frac{d\Gamma}{dx_b} = \delta(1-x_b) + \frac{\alpha_S(\mu)}{2\pi}\left[P_{qq}(x_b)\ln\frac{Q^2}{m_b^2} + A(x_b)\right] + \mathcal{O}\left(\frac{m_b^2}{Q^2}\right)^p. \tag{3}$$

In Eq. (3), x_b is the normalized b-quark energy fraction:

$$x_b = \frac{1}{1-w}\frac{2p_b\cdot Q}{Q^2}, \tag{4}$$

where $w = 0$ in Z and H decay, and $w = m_W^2/m_t^2$ in top decay, since the W mass is not negligible with respect to the top mass. Furthermore, in Eq. (3) Γ_0 is the width of the Born process, μ is the renormalization scale, $p \geq 1$, $P_{qq}(x_b)$ is the Altarelli–Parisi splitting function:

$$P_{qq}(x_b) = C_F\left(\frac{1+x_b^2}{1-x_b}\right)_+. \tag{5}$$

Function $A(x_b)$ is process-dependent and does not contain the b mass.

The large logarithm $\ln(Q^2/m_b^2)$, which appears in Eq. (3), can be resummed following the approach of perturbative fragmentation functions [10]. The b spectrum is expressed as the convolution of a massless coefficient function and a perturbative fragmentation function $D(m_b,\mu_F)$, associated with the transition of a massless parton into a heavy quark:

$$\begin{aligned}\frac{1}{\Gamma_0}\frac{d\Gamma_b}{dx_b}(x_b,Q,m_b) &= \sum_i \int_{x_b}^1 \frac{dz}{z}\left[\frac{1}{\Gamma_0}\frac{d\hat{\Gamma}_i}{dz}(z,Q,\mu,\mu_F)\right]^{\overline{\rm MS}} D_i^{\overline{\rm MS}}\left(\frac{x_b}{z},\mu_F,m_b\right)\\ &+ \mathcal{O}\left((m_b/Q)^p\right)\,.\end{aligned} \tag{6}$$

In Eq. (6), $d\hat{\Gamma}_i/dz$ is the differential width for the production of a massless parton i in any of the considered processes, after subtraction of the collinear singularity in the $\overline{\rm MS}$ factorization scheme. Throughout this paper, and for all the considered processes, we shall neglect secondary b-quark production via $g \to b\bar{b}$ splitting, which means that, in Eq. (6), $i = b$ and $D_b^{\overline{\rm MS}}$ expresses the fragmentation of a massless b into a massive b. The NLO $\overline{\rm MS}$ coefficient functions were calculated in [10, 16, 18] for Z, t and H decays respectively.

The perturbative fragmentation function follows the DGLAP evolution equations [11, 12]. Its value at a given scale μ_F can be obtained once an initial condition is given.

In [10] the initial condition $D_b^{\rm ini}(x_b, \mu_{0F}, m_b)$ was calculated and its process-independence was established on more general grounds in [13]. It is given at NLO by:

$$D_b^{\rm ini}(x_b, \mu_{0F}, m_b) = \delta(1-x_b) + \frac{\alpha_S(\mu_0^2) C_F}{2\pi} \left[\frac{1+x_b^2}{1-x_b} \left(\ln \frac{\mu_{0F}^2}{m_b^2} - 2\ln(1-x_b) - 1 \right) \right]_+ . \quad (7)$$

As discussed in [10], solving the DGLAP equations for an evolution from μ_{0F} to μ_F, with a NLO kernel, allows one to resum leading (LL) $\alpha_S^n \ln^n(\mu_F^2/\mu_{0F}^2)$ and next-to-leading (NLL) $\alpha_S^n \ln^{n-1}(\mu_F^2/\mu_{0F}^2)$ logarithms (collinear resummation). The explicit expression for the solution of the DGLAP equations can be found, for instance, in Ref. [10]. Setting $\mu_{0F} \simeq m_b$ and $\mu_F \simeq Q$, one resums the large $\ln(Q^2/m_b^2)$ appearing in the massive spectrum (3).

The NNLO initial condition of the perturbative fragmentation function was calculated in Refs. [29, 30]; however, for the NNLO result to be applicable, one would also need three-loop time-like splitting functions, which are currently unknown.

Furthermore, both the initial condition (7) and the coefficient functions in [10,16,18] present terms, $\sim 1/(1-x_b)_+$ and $\sim [\ln(1-x_b)/(1-x_b)]_+$, which become large for $x_b \to 1$. The large-x_b limit corresponds to soft-gluon radiation; in Mellin moment space, such terms correspond, at $\mathcal{O}(\alpha_S)$, to single ($\sim \alpha_S \ln N$) and double ($\sim \alpha_S \ln^2 N$) logarithms of the Mellin variable N. Soft resummation in the initial condition of the perturbative fragmentation function is process-independent and was performed in [13] in the NLL approximation. Large-x_b resummation in the coefficient functions was implemented in [13] for e^+e^- annihilation, in [17] for top decay, in [18] for $H \to b\bar{b}$ processes. In N-space and in the NLL approximation, terms $\sim \alpha_S^n \ln^{n+1} N$ (LL) and $\sim \alpha_S^n \ln^n N$ (NLL) are kept in the Sudakov exponent.

The soft and collinear resummations in [13, 17, 18] are matched to the exact NLO results, in order to give a reliable prediction over the full x_b (N) range. This implies that the total widths are NLO as well.

It was shown in Refs. [13, 17, 18] that, after soft and collinear logarithms are resummed, the b-quark spectra present very little dependence on factorization and renormalization scales, which is equivalent to saying that the theoretical uncertainty is reduced. Hereafter, we shall set the scales appearing in Eqs. (6) and (7) to: $\mu = \mu_F = Q$, $\mu_0 = \mu_{0F} = m_b$.

3 Parton shower algorithms

In this section we discuss parton shower algorithms, as implemented in Monte Carlo event generators, such as HERWIG and PYTHIA. These algorithms rely on the universality of the elementary branching probability in the soft or collinear approximation. Referring, for simplicity, to final-state radiation, the probability of emission of a soft or collinear parton reads:

$$dP = \frac{\alpha_S}{2\pi}\frac{dQ^2}{Q^2}\ \hat{P}(z)\ dz\ \frac{\Delta_S(Q^2_{\rm max}, Q^2)}{\Delta_S(Q^2, Q^2_0)}. \tag{8}$$

In (8), $\hat{P}(z)$ is the tree-level Altarelli–Parisi splitting function [1], z is the energy fraction of the emitted parton with respect to the emitter, Q^2 is the ordering variable of the shower. In HERWIG [19], Q^2 is an energy-weighted angle [2], which corresponds to angular ordering in the soft limit [31]. In PYTHIA [20], Q^2 is the momentum squared of the radiating parton, with an option to veto branchings that do not fulfil the angular ordering prescription. Moreover, the latest version of it, PYTHIA 6.3 [21], offers as an alternative the possibility to order final-state showers according to the transverse momentum of the emitted parton with respect to the emitter's direction, along the lines of [32]. For most of the results that we shall present, we shall use PYTHIA 6.220, with the option to reject non-angular-ordered showers turned on, and HERWIG 6.506 [33].

In (8) $\Delta_S(Q^2_1, Q^2_2)$ is the Sudakov form factor, expressing the probability of evolution from Q^2_1 to Q^2_2 with no resolvable emission. In particular, the ratio of form factors in (8) represents the probability that the considered emission is the first, i.e. there is no emission between Q^2 and $Q^2_{\rm max}$, where $Q^2_{\rm max}$ is set by the hard-scattering process. Q^2_0 is instead the value of Q^2 at which the shower evolution is terminated. In diagrammatic terms, the Sudakov form factor sums up all virtual and unresolved real emissions to all orders.

For multiparton radiation, iterating the branching probability (8) is equivalent to performing the resummation of soft- and collinear-enhanced radiation. As discussed, for example, in [34] in the framework of the HERWIG event generator, parton shower algorithms resum leading logarithms in the Sudakov exponent, and include a class of subleading NLLs as well.

Standard Monte Carlo event generators yield the leading-order total cross section for all implemented processes. The more recent 'Monte Carlo at next-to-leading order'

[1] Unlike Eq. (5), which includes virtual corrections as well, in Eq. (8) $\hat{P}(z)$ only accounts for real, small-angle parton radiation. We have, for example, $\hat{P}_{qq}(z) = C_F(1+z^2)/(1-z)$, without the plus prescription appearing in Eq. (5).

[2] In the HERWIG showering frame, $Q^2 \simeq E^2(1-\cos\theta)$, where E is the energy of the splitting parton and θ is the emission angle [31].

(MC@NLO) [35] program implements instead both real and virtual corrections to the hard-scattering process, in such a way that predicted observables, including total cross sections, are correct to NLO accuracy.

While resummed calculations typically do not implement the widths of the decaying particles, whose masses are fixed quantities in the calculations, Monte Carlo generators include the finite widths of Z, W, Higgs bosons and top quarks. Some discussion on width effects will be presented in section 6, when we shall investigate the decay of a Higgs boson with a mass of 500 GeV.

Moreover, for Higgs or top quark events, both HERWIG and PYTHIA neglect interference effects between production and decay phases. In this approximation, the differential decay width, normalized to the total width, is equal to the normalized differential cross section, independently of the production process:

$$\frac{1}{\Gamma}\frac{d\Gamma}{dx_b} = \frac{1}{\sigma}\frac{d\sigma}{dx_b}. \tag{9}$$

Neglecting interference is a reliable approximation, as long as the energies of the radiated gluons are much larger than the top or Higgs widths [36]. This is indeed the case whenever the experimental analyses set cuts, e.g. on the transverse momenta of the reconstructed jets in top-quark events, of the order of 10 GeV or larger. Although not really essential in view of Eq. (9), in the following we shall nonetheless run HERWIG and PYTHIA for top and Higgs production at the LHC, i.e. for pp collisions at a centre-of-mass energy $\sqrt{s} = 14$ TeV.

4 Matrix-element corrections to parton showers

The algorithm briefly discussed in the previous section is able to simulate soft or collinear radiation; for hard and large-angle emission, the exact matrix element must be used. In fact, Monte Carlo parton showers are supplemented by matrix-element corrections.

PYTHIA uses the soft/collinear approximation in all the physical phase space and the exact tree-level matrix element corrects the first emission [23,37]. In particular, PYTHIA 6.220 contains matrix-element corrections to all processes that we shall investigate.

The standard HERWIG algorithm entirely suppresses radiation in the so-called 'dead zone' of the phase space, corresponding to hard and large-angle emission. The exact matrix element is used to populate the dead zone (hard correction) and to correct the shower every time an emission is capable of being the 'hardest so far' (soft correction), i.e. the emitted parton has the largest transverse momentum with respect to the emitting one [22]. HERWIG 6.506 [33] contains matrix-element corrections to e^+e^- annihilation

[38], Deep Inelastic Scattering [39], top decay [40] and vector-boson production [41]. The corrections to Higgs hadroproduction ($gg/q\bar{q} \to H$), whose inclusion is in progress, are discussed in [42]. In this section, we shall briefly discuss the implementation of matrix-element corrections to parton showers in $H \to b\bar{b}$ decays, not yet present in HERWIG.

As the Higgs is a colourless particle, the corrections to $H \to b\bar{b}$ are a straightforward extension of the ones to $Z \to b\bar{b}$ processes [38]. The limits of the phase-space region populated by HERWIG will be exactly the ones computed in [38], with m_H replacing m_Z. The total and HERWIG's phase spaces are plotted in Fig. 1, in terms of x_b and $x_{\bar{b}}$. Collinear, corresponding to either $x_b = 1$ or $x_{\bar{b}} = 1$, and soft emissions, i.e. the point $x_b = x_{\bar{b}} = 1$, are within the HERWIG phase space; no radiation is allowed in the dead zone. We also note an overlapping region, where radiation may come from either b or $\bar{b}$.

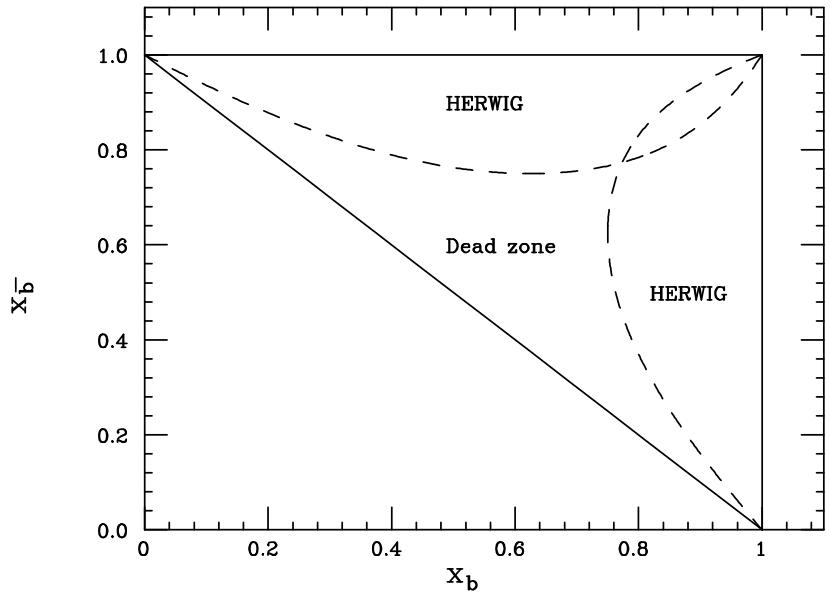

Figure 1: Total (solid) and HERWIG (dashes) phase spaces for gluon radiation in $H \to b\bar{b}$ processes. The dead zone is empty in the standard algorithm.

To implement matrix-element corrections, we need to compute the double-differential width of $H \to b\bar{b}g$ processes, corresponding to the Feynman diagrams in Fig. 2, in terms of the b and $\bar{b}$ energy fractions. It reads:

$$\frac{1}{\Gamma_0}\frac{d^2\Gamma}{dx_b\, dx_{\bar{b}}} = \frac{\alpha_S C_F}{2\pi}\, \frac{x_b^2 + x_{\bar{b}}^2 + 2x_b x_{\bar{b}} - 2x_b - 2x_{\bar{b}} + 2}{(1-x_b)(1-x_{\bar{b}})}. \tag{10}$$

In Eq. (10) the scale of α_S is set to the gluon transverse momentum with respect to the direction of the emitting quark: this choice is suitable to sum up a class of next-

to-leading logarithmic corrections [15]. When applying matrix-element corrections, we generate events in the dead zone according to Eq. (10), and use the exact result to correct the cascade in the already-populated region, any time an emission is the hardest so far. We have estimated that, after matrix-element corrections are applied, for a Higgs mass $m_H = 120$ GeV, about 4% of events have a gluon emission in the dead zone. For $m_H = 500$ GeV, this fraction becomes about 3%, since, for a larger mass value, even the gluon transverse momentum q_T^2 is on average larger and therefore $\alpha_S(q_T^2)$ smaller.

Figure 2: Feynman diagrams for $H \to b\bar{b}g$.

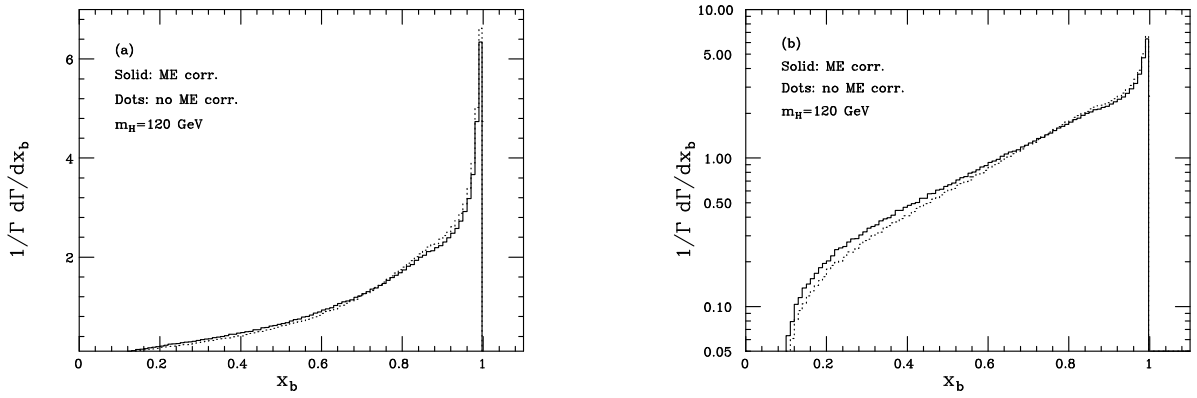

Figure 3: b-quark energy spectrum in Higgs decay, according to HERWIG with (solid) and without (dotted) matrix-element corrections, on linear (a) and logarithmic (b) scales, for $m_H = 120$ GeV.

Figures 3–4 show the effect of matrix-element corrections on the b-quark energy fraction, for $m_H = 120$ and 500 GeV, the values that we will consider in the following. As expected, more events are generated at small x_b (corresponding to the dead zone of the standard algorithm) through the exact amplitude; this enhancement is compensated by having less events at large x_b. In fact, even after matrix-element corrections are applied, HERWIG, as well as PYTHIA, gives by default the total leading-order cross

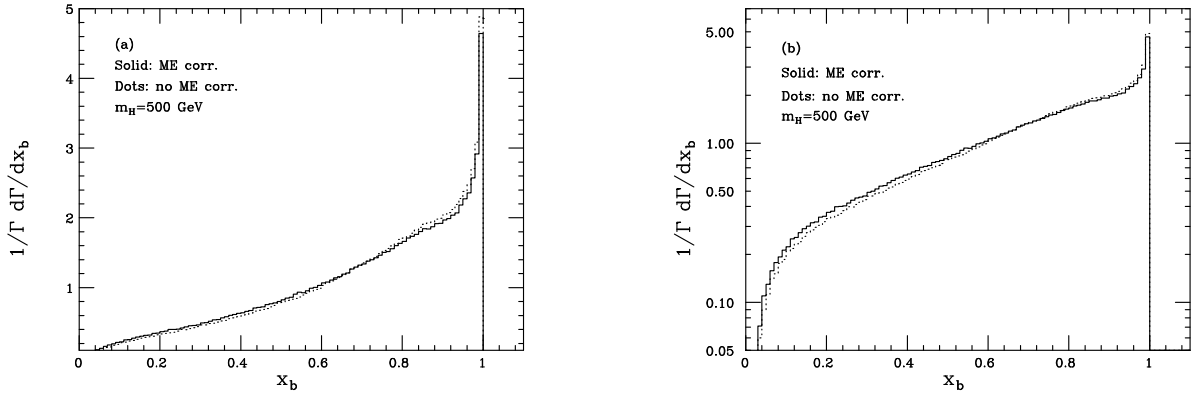

Figure 4: As in Fig. 3, but for a Higgs mass $m_H = 500$ GeV.

sections (widths). We also observe that the x_b spectra present a sharp peak for $x_b \to 1$, which corresponds to events where no gluon is emitted by the $b\bar{b}$ pair ($x_b = x_{\bar{b}} = 1$). The fraction of events with $x_b = 1$ depends on the shower cutoff Q_0 in Eq. (8), a user-defined parameter of HERWIG [19].

5 B-hadron spectrum in x_B-space

In this section we wish to present results on the B-hadron spectrum in e^+e^- annihilation, Higgs and top decay. Our tools to describe b-quark production will be, as discussed above, NLL-resummed calculations, HERWIG and PYTHIA. Given the different perturbative accuracies, treatment of width effects and hadronization models which are implemented, we do not expect that NLL computations and Monte Carlo event generators should necessarily agree. However, we find it very interesting to perform this comparison, since they are tools that are used for the analyses of b-quark fragmentation, and it is useful to estimate the quality of the agreement between the predictions they make. Since the description of perturbative b production is different, in order for our comparison to be consistent, we shall have to tune independently HERWIG, PYTHIA and the hadronization model used in the framework of resummed calculations to the same data set. Such a consistency is crucial if we wish to extract non-perturbative information from e^+e^- annihilation and use it to predict B-hadron production in other processes [26, 50].

In order to describe B-hadron spectra in the considered processes, we use experimental data on B production in e^+e^- annihilation, and rely on the universality of the hadronization mechanism. We shall account for data from SLD [1] and from the LEP experiments ALEPH [2] and OPAL [3] [3]. Our results will be expressed in terms of the

[3]Contrary to Refs. [16–18], here we consider the OPAL data too.

B normalized energy fraction x_B, which is the hadron-level counterpart of Eq. (4):

$$x_B = \frac{1}{1-w}\frac{2p_B \cdot Q}{Q^2}, \tag{11}$$

where p_B is the B four-momentum. As pointed out in section 2, when we use a resummed calculation that neglects powers of m_b^2/Q^2, $w = m_W^2/m_t^2$ for top decay, while $w = 0$ for the other processes. Since Monte Carlo event generators include some m_b^2/Q^2 effects, $w = m_W^2/m_t^2 - m_b^2/m_t^2$ for top decays in HERWIG and PYTHIA.

ALEPH and OPAL reconstructed only weakly-decaying B mesons, while the SLD sample contains some B baryons too; however, since the fraction of baryons is pretty small, we can safely fit all data together and, when running HERWIG or PYTHIA, we shall account for both mesons and baryons. As the resummed calculation yields a NLO total cross section (width), and the considered Monte Carlo programs only the LO one, we shall study normalized distributions, such as $1/\Gamma\ d\Gamma/dx_B$, everywhere.

As far as the NLL resummed calculation is concerned, up to power corrections, one writes the hadron-level spectrum as the convolution of the parton-level one, determined as discussed in Section 2, with a non-perturbative fragmentation function:

$$\frac{1}{\Gamma}\frac{d\Gamma_B}{dx_B}(x_B, Q, m_b) = \frac{1}{\Gamma}\int_{x_B}^1 \frac{dz}{z}\frac{d\Gamma_b}{dz}(z, Q, m_b) D^{\rm np}\left(\frac{x_B}{z}\right). \tag{12}$$

We describe the hadronization using the Kartvelishvili non-perturbative fragmentation function [24]:

$$D^{\rm np}(x;\gamma) = (1+\gamma)(2+\gamma)(1-x)x^\gamma, \tag{13}$$

and fit the free parameter γ to the data. As in [16–18], we consider the data in the range $0.18 \le x_B \le 0.94$, to avoid the regions $x_B \to 0$ and $x_B \to 1$, where the calculation is unreliable. In fact, the parton- and hadron-level spectra presented in [13,16–18] become negative at very small and very large x, which is due to the presence of terms that have not been resummed yet, and to non-perturbative corrections, relevant especially at large x. When doing the fit, we set the scales in Eqs. (6) and (7) and the parameters entering the perturbative calculation to the following values: $\mu = \mu_F = m_Z$, $\mu_0 = \mu_{0F} = m_b$, $m_Z = 91.188$ GeV, $m_b = 5$ GeV, $\Lambda^{(5)}_{\overline{\rm MS}} = 200$ GeV. In the considered range, we obtain: $\gamma = 17.178 \pm 0.303$, with $\chi^2/{\rm dof} = 46.2/53$ from the fit.

If we try to compare the data with the considered Monte Carlo generators, we find that the default parametrizations of the hadronization models in HERWIG and PYTHIA are not able to reproduce the x_B data. The χ^2 per degree of freedom are, in fact, $\chi^2/{\rm dof} = 739.4/61$ for HERWIG and $\chi^2/{\rm dof} = 467.9/61$ for PYTHIA. A fit of HERWIG to a number of observables in e^+e^- annihilation was performed in [43]. Employing the parameters suggested in [43] gives $\chi^2/{\rm dof} = 391.9/61$ for the comparison with the x_B data.

In this paper we wish to reconsider the tuning of HERWIG and PYTHIA to the b-fragmentation data. We point out that we are aware of the fact that care must be

taken when changing the parameters of a Monte Carlo event generator, since this may spoil the agreement with the data sets that were used in the default tuning. The fits that we shall perform should not be seen as an attempt to redefine the parameters of HERWIG or PYTHIA; we would just like to investigate whether it is possible to change few parameters to describe the x_B data better. Of course, it will be interesting to use the parametrization which we shall suggest to check how HERWIG and PYTHIA fare with respect to other observables. When doing the tuning, we concentrate on the parameters that determine the hadronization and leave unchanged the ones related to the perturbative phase of the showers and the quark masses.

In HERWIG, we modify the values of CLSMR(1) and CLSMR(2), controlling the Gaussian smearing of the hadron direction with respect to the original constituent quarks; PLSPLT(2), which determines the mass distribution of b-flavoured cluster decays; DECWT, affecting the relative weight of decuplet and octet baryons; and CLPOW, to which the heavy-cluster yield and the baryon/meson ratio are sensitive. The fitted values are: CLSMR(1) = 0.4 (default 0), CLSMR(2) = 0.3 (0), PSPLT(2) = 0.33 (1), DECWT = 0.7 (1), CLPOW = 2.1 (2). The values of CLSMR(1), PSPLT(2) and DECWT are indeed the same as in Ref. [43]. After the tuning, the agreement with the data is still not very good, but it is much better than with the default parametrization. We find $\chi^2/\mathrm{dof} = 222.4/61$.

As for PYTHIA, we change the values of the fragmentation parameters PARJ(41) and PARJ(42), which control the a and b parameters of the Lund symmetric fragmentation function [4]:

$$f_L(z) \propto \frac{1}{z}(1-z)^a \exp(-bm_T^2/z). \tag{14}$$

We also tune PARJ(46), which modifies the endpoint of the Lund function according to the Bowler hadronization model [46] [5]:

$$f_B(z) \propto \frac{1}{z^{1+bm_q^2}}(1-z)^a \exp(-bm_T^2/z), \tag{15}$$

where m_q is the quark mass. Our tuning gives the following values: PARJ(41) = 0.85 (default value 0.3), PARJ(42) = 1.03 (0.58), PARJ(46) = 0.85 (1). After our tuning, PYTHIA matches the e^+e^- data well, and we obtain $\chi^2/\mathrm{dof} = 45.7/61$ from the fit. In Table 1 we summarize the parameters of HERWIG and PYTHIA that we have changed in our tuning. We have checked that our tuning works well also for the new model implemented in PYTHIA 6.3, as long as one runs it using options and parameters as they are defined in the new scenario (model 1) [47]. Running PYTHIA 6.3, we find $\chi^2/\mathrm{dof} = 46.0/61$ for the comparison with the x_B data. In Figs. 5-6 we compare LEP and SLD data with HERWIG and PYTHIA respectively, using the default and tuned parameters. In both figures, we also show the results given by the resummed calculations of Ref. [13], convoluted with the Kartvelishvili model (solid), and denoted

[4] For a quark of energy E moving on the z axis, the quantity z appearing in Eq. (14) is the fraction of $E + p_z$ taken by the hadron, while m_T is transverse mass, i.e. $m_T^2 = m^2 + p_x^2 + p_y^2$.

[5] See also the PYTHIA manual [20] for details on the implementation of Eqs. (14) and (15).

Table 1: Parameters of HERWIG and PYTHIA hadronization models that we have tuned to improve the agreement with e^+e^- data, along with the χ^2 per degree of freedom.

HERWIG	PYTHIA
CLSMR(1) = 0.4	
CLSMR(2) = 0.3	PARJ(41) = 0.85
DECWT = 0.7	PARJ(42) = 1.03
CLPOW = 2.1	PARJ(46) = 0.85
PSPLT(2) = 0.33	
χ^2/dof = 222.4/61	χ^2/dof = 45.7/61

by 'NLO+NLL+Kart.' For the sake of comparison, we present the PYTHIA spectrum obtained using the parameters of Table 1, but without the rejection of non-angular-ordered showers.

The x_B distributions given by HERWIG and PYTHIA with the default parameters deviate significantly from the data points, as suggested by the χ^2 values. The NLO+NLL calculation and PYTHIA after the tuning describe the data quite well. If we turn angular ordering off, PYTHIA is obviously not capable of reproducing the data. In fact, when tuning PYTHIA, we have used a version that vetoes non-angular-ordered-showers; if we allow non-angular-ordered branchings in PYTHIA, we should in principle even reconsider the tuning. Besides the comparison with the data, it is nonetheless interesting to observe the effect of possible non-angular-ordered showers: more events in the middle–low range $0.2 \lesssim x_B \lesssim 0.6$ and less events around the peak. In the following, we shall always run PYTHIA with forced angular ordering.

The distribution yielded by HERWIG is instead somewhat broader than the data set. Even after the tuning, HERWIG is above the data at small and large x_B and below the data in the neighbourhood of the peak. In any case, the comparison is greatly improved with respect to the default parametrization, and in principle even the HERWIG parameters which control perturbative b production can be further tuned. Furthermore, major improvements in the treatment of b fragmentation are present in HERWIG++ [44], the new object-oriented C++ version, which uses new showering variables and includes quark masses in the splitting functions [45]. As discussed in [44], one can obtain a quite good description of the SLD x_B data fitting only the shower cutoff, corresponding to Q_0 in Eq. (8), and without any additional tuning of the hadronization model. The use of HERWIG++, whose first version simulates e^+e^- annihilation, is however beyond the scope of this paper.

Relying on the universality of the hadronization mechanism, we can use the parametriza-

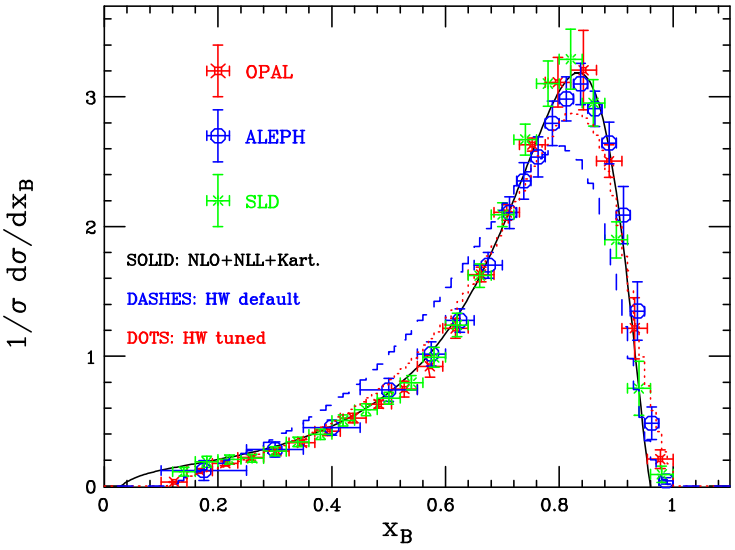

Figure 5: Data from LEP and SLD experiments, compared with the NLO+NLL calculation convoluted with the Kartvelishvili model (solid) and HERWIG 6.506, using the default parametrization (dashed) and our tuning (dotted).

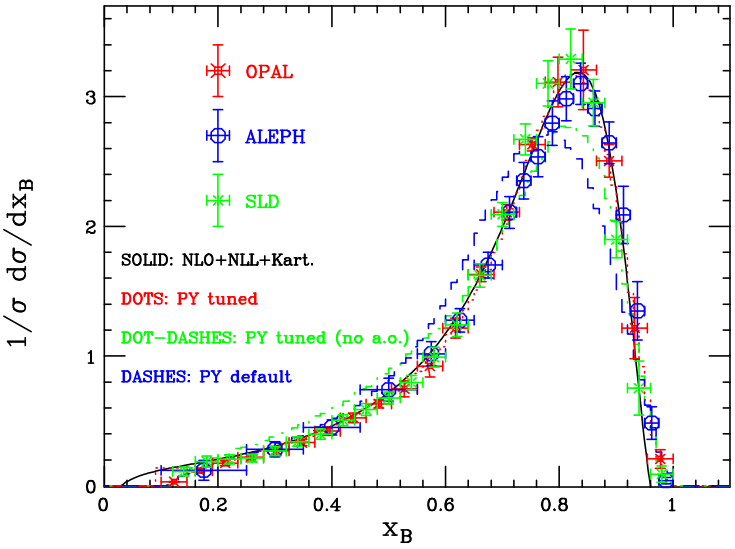

Figure 6: As in Fig. 5, but comparing data and the NLO+NLL calculation with default (dashed) and tuned (dotted) PYTHIA 6.220. Also shown is the PYTHIA prediction, using our tuning of the hadronization model, but without rejecting the showers which do not fulfil angular ordering (dot-dashed).

tions quoted in Table 1 to predict the x_B distribution in $H \to b\bar{b}$ and $t \to bW$. In Higgs decay we shall investigate the cases $m_H = 120$ and 500 GeV; in top decay we shall assume $m_t = 175$ GeV and $m_W = 80.425$ GeV. The other quantities will be set consistently with the values employed in the fit to the e^+e^- data.

In Fig. 7, we plot the B-hadron spectrum in $H \to b\bar{b}$ processes, using HERWIG,

PYTHIA, and the NLL-resummed calculation in [18], convoluted with the Kartvelishvili model fitted as above. We have set the Higgs mass to $m_H = 120$ GeV. PYTHIA fares rather well with respect the NLO+NLL calculation: although small discrepancies are present at very small and large x_B and around the peak, the overall agreement looks acceptable. The behaviour of the curves given by HERWIG reflects what we found in the comparison with the e^+e^- data: even in Higgs decay, the x_B spectrum is broader, lies above the NLO+NLL computation at large and intermediate x_B, and below around the peak. Since matrix-element corrections to $e^+e^- \to b\bar{b}$ were included when we did the fit, in principle the tuned parameters must be used only when matrix-element corrections to $H \to b\bar{b}$ are turned on. However, for the sake of comparison, we show in Fig. 7 the x_B spectrum given by HERWIG without such corrections as well. The effect of matrix-element corrections is indeed what one should expect: we have more events at small x_B, say $x_B < 0.6$, and less at large x_B. In fact, as shown in Figs. 3 and 4, the implementation of hard and large-angle gluon radiation enhances the probability to have b quarks with smaller x_b, since the gluon is allowed to take a larger energy fraction. It is therefore reasonable that this is reflected by having more hadrons at small x_B as well.

We would like to consider also the case of a Higgs with a very large mass, in particular $m_H = 500$ GeV. This example does not have a relevant application in the Standard Model, where the branching ratio of $H \to b\bar{b}$ is tiny for such a high-mass value, but it could become more important in models with an extended Higgs sector. Another interesting aspect is to investigate whether our predictions are still in reasonable agreement for masses well above the Z-boson mass. For $m_H = 500$ GeV, width effects may become important; however, for the sake of comparison with the resummed calculation, which does not implement the Higgs width, we run HERWIG and PYTHIA for $\Gamma_H = 0$. The spectra shown in Fig. 8 look broader than the 120 GeV case, but the comparison is rather similar: PYTHIA yields the highest spectrum at small x_B and HERWIG at intermediate and very large x_B. The effects of matrix-element corrections to $H \to b\bar{b}$ in HERWIG has an impact that is similar to the one already observed if Fig. 7: more events at small x_B and less around the peak. We have finally checked that the impact of the inclusion of finite-width effects in HERWIG and PYTHIA is of the order of 1%.

In Fig. 9, we compare the B-hadron spectrum in top-quark decay, using HERWIG, PYTHIA and the perturbative NLO+NLL resummed calculation performed in [16, 17], convoluted with the Kartvelishvili non-perturbative model. PYTHIA is able to reproduce rather well the peak given by the resummed calculation, while its spectrum lies below it at $x_B \lesssim 0.7$ and above it at $x_B \gtrsim 0.95$. The spectrum given by HERWIG looks instead slightly different: it is below the resummed calculation in most of the x_B range, i.e. $x_B \lesssim 0.9$, and above at very large x_B.

In [18] the B spectra in Z, top and Higgs decays were compared using NLL resummed calculations. In Figs. 10 and 11 we show the same comparison, but running HERWIG and PYTHIA; in order to investigate the effect of the particle spins, we also show the result in e^+e^- annihilation, but for $\sqrt{s} = 120$ GeV, the chosen value for the Higgs mass. Figs. 10 and 11 exhibit features similar to those of Ref. [18]: the B energy distribution in

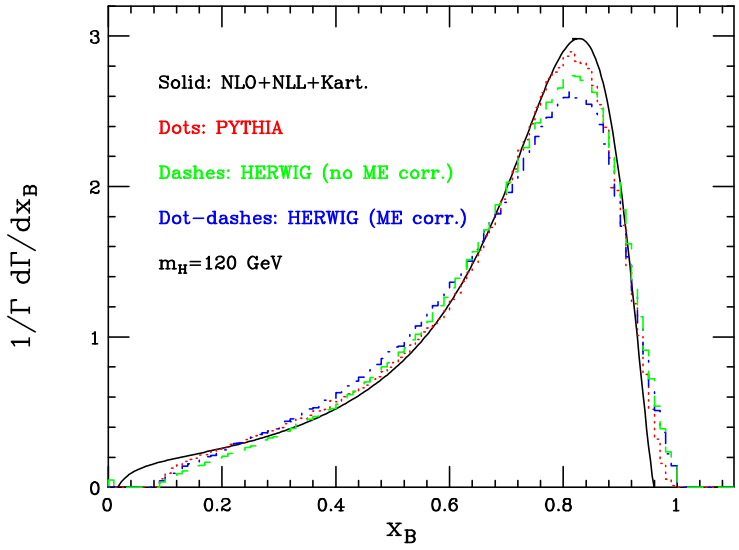

Figure 7: B-hadron spectra in $H \to b\bar{b}$ processes, according to a NLO+NLL calculation with the Kartvelishvili non-perturbative model (solid line), PYTHIA (dotted) and HERWIG with (dot-dashed) and without (dashed) matrix-element corrections. We have set $m_H = 120$ GeV and used the tuning in Table 1.

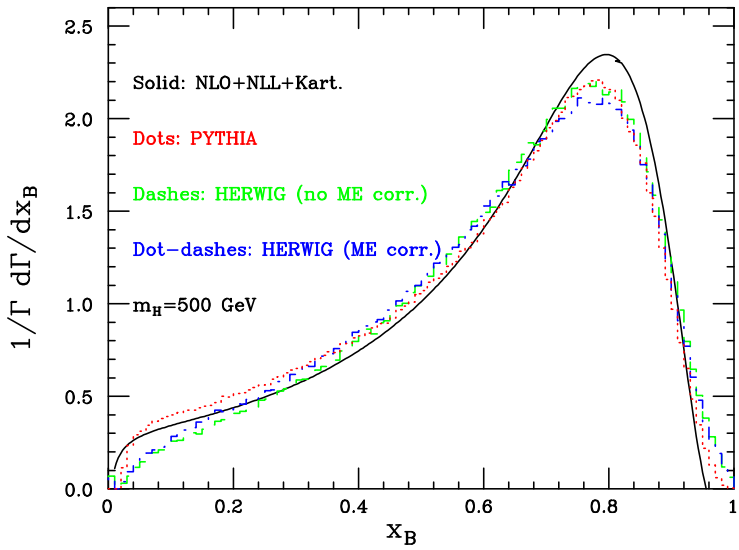

Figure 8: As in Fig. 7, but for a Higgs mass $m_H = 500$ GeV, and with no width effects in HERWIG and PYTHIA.

top decay is shifted toward large x_B values; in Higgs decay we have more events at small x_B; the spectrum from Z decay lies between the two. Setting $m_Z = m_H$, as observed in [18], makes the spectra from H and Z decays more similar, but small discrepancies are still present. The comparison between top and Higgs decays is indeed quite relevant, since the different B spectra may help to distinguish between b-flavoured hadrons in the process $pp \to t\bar{t}H$, followed by $H \to b\bar{b}$, one of the most important channels for Higgs studies at the LHC [7].

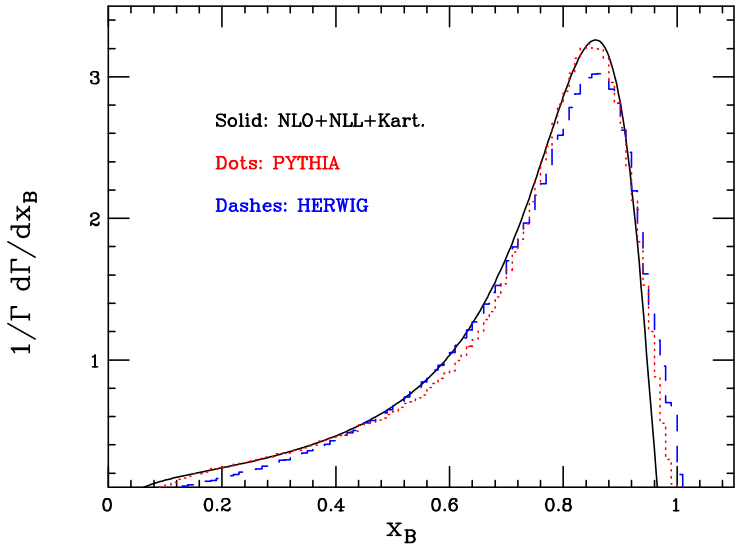

Figure 9: B-hadron spectra in top decay, for $m_t = 175$ GeV, according to a NLO+NLL computation convoluted with the Kartvelishvili model, (solid line), HERWIG (dashed) and PYTHIA (dotted).

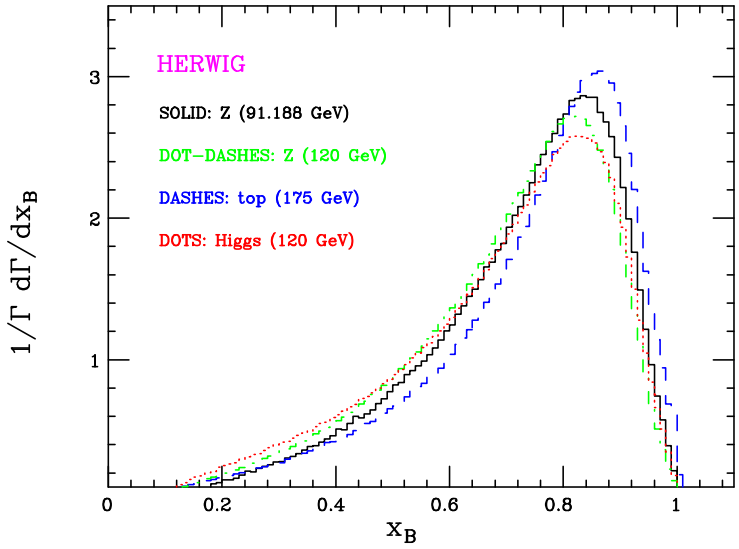

Figure 10: Comparison of B-hadron spectra in $Z \to b\bar{b}$ for $m_Z = 91.188$ GeV (solid) and $m_Z = 120$ GeV (dot-dashed), for top decay (dashed) and for $H \to b\bar{b}$ (dotted), with $m_H = 120$ GeV. Results given by HERWIG, with matrix-element corrections included in all plots.

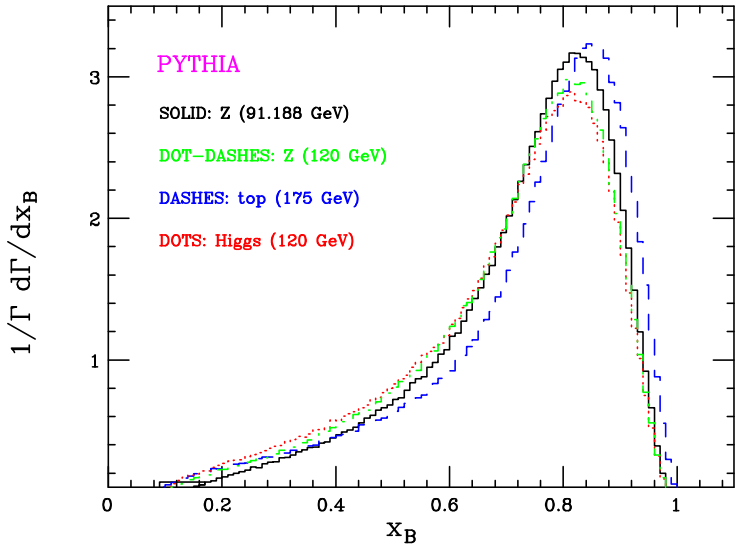

Figure 11: As in Fig. 10, but using PYTHIA.

6 Results in moment space

In this section we wish to present results in moment space, where the moments Γ_N of a function $1/\Gamma\ d\Gamma/dz$ are defined as follows:

$$\Gamma_N = \int_0^1 dz\ z^{N-1} \frac{1}{\Gamma} \frac{d\Gamma}{dz}(z). \tag{16}$$

In the case of the histograms given by a Monte Carlo program, the integral in (16) will be approximated to a discrete sum over the bins. In Ref. [48], the DELPHI collaboration presented the moments for B production in e^+e^- annihilation. From the point of view of resummed calculations, working in moment space [26,49] presents several advantages. In N-space, convolutions become ordinary products, and the relation between parton- and hadron-level cross sections becomes:

$$\sigma_N^B = \sigma_N^b D_N^{\rm np}, \tag{17}$$

where σ_N^b and σ_N^B are the moments of the b and B cross sections, and $D_N^{\rm np}$ the N-space counterpart of the non-perturbative fragmentation function. Therefore, there is no need to assume any functional form for the non-perturbative fragmentation function in x space. Moreover, resummed calculations are well defined in N-space, and we do not have the problem exhibited by the x_B-space spectra, which become negative at small or large x_B.

In [17,18], the parton- and hadron-level moments for $t \to bW$ and $H \to b\bar{b}$ processes were presented, using a resummed NLL perturbative calculation. In this paper, we wish to compare experimental data and predictions, employing HERWIG and PYTHIA as well, tuned as in Table 1.

In Table 2 we quote the data from DELPHI, the moments yielded by HERWIG and PYTHIA in Z, t and H decays, and, for the sake of comparison, the results, already published in [17,18], yielded by NLL-resummed calculations. As for the NLL computation, we present two sets of results: we multiply the moments of the perturbative cross sections (widths) by the moments of the Kartvelishvili model, denoted by K_N in Table 2, fitted to LEP and SLD x_B-space data, and by $D_N^{\rm np}$, extracted from the DELPHI N-space data [48]. The moments yielded by HERWIG and PYTHIA in e^+e^- annihilation are consistent, within the error ranges, with the ones measured by DELPHI. Although problems are present when fitting the x_B data from LEP and SLD, it is remarkable that HERWIG is compatible with the DELPHI moments within one standard deviation. Moreover, we observe that the moments given by the NLL calculation are rather different according to whether the fit is made directly to the N-space DELPHI data, or by fitting in x_B space and then calculating the moments. In fact, the x_B-space fit was performed in the range $0.18 \leq x_B \leq 0.94$, while the moments are computed integrating over the full range $0 \leq x_B \leq 1$. Neglecting data at small and large x_B in the fit may cause an incorrect determination of the moments, which do depend on the tails of the distributions [26, 49].

The results for top and Higgs decay exhibit similar features to the x_B spectra. In top decay, PYTHIA is very close to the NLL calculation which uses $D_N^{\rm np}$ extracted from the DELPHI data, while HERWIG, whose predictions are shifted toward larger x_B, gives larger moments. For $H \to b\bar{b}$ and $m_H = 120$ GeV, PYTHIA and HERWIG, after matrix-element corrections, give moments which are compatible within 1%, and are closer to the NLL result which uses the Kartvelishvili model rather than the moments $D_N^{\rm np}$. For $m_H = 500$ GeV, HERWIG looks somewhat closer to the NLL result, while PYTHIA gives moments which are a few per cent smaller. Matrix-element corrections to $H \to b\bar{b}$ in HERWIG have the effect to reduce the values of the moments of about 2–5% for both $m_H = 120$ and 500 GeV, which is understandable, since more small-x_B events are generated after the inclusions of such corrections.

7 Conclusions

We have studied bottom-quark fragmentation in e^+e^- annihilation, as well as in top and Higgs decay, using NLL-resummed calculations based on the fragmentation function formalism and Monte Carlo event generators, such as HERWIG and PYTHIA. Monte Carlo parton showers simulate multiple radiation in the soft or collinear approximation, and need to be provided with matrix-element corrections to simulate hard and large-angle parton radiation. While PYTHIA contained the corrections to all three considered processes, we had to implement matrix-element corrections to $H \to b\bar{b}$ in HERWIG, since they are not yet present in HERWIG. At parton level, the effect of such corrections is that there are more b quarks simulated with a smaller energy fraction.

We have fitted HERWIG, PYTHIA and the Kartvelishvili hadronization model, the

Table 2: Moments σ_N^B from DELPHI [48], and moments in e^+e^- annihilation, Higgs (H) and top (t) decay, using NLL resummed calculations, HERWIG (HW) and PYTHIA (PY). In $H \to b\bar{b}$, we consider the Higgs mass values $m_H = 120$ GeV and 500 GeV, and quote HERWIG results with (c.) and without (no c.) matrix-element corrections. The NLL results are obtained by extracting $D_n^{\rm np}$ from the DELPHI data, and using the moments K_N of the Kartvelishvili model, fitted to x_B data, as in Figures 5 and 6.

	$\langle x \rangle$	$\langle x^2 \rangle$	$\langle x^3 \rangle$	$\langle x^4 \rangle$
e^+e^- data σ_N^B	0.7153±0.0052	0.5401±0.0064	0.4236±0.0065	0.3406±0.0064
e^+e^- NLL σ_N^b	0.7801	0.6436	0.5479	0.4755
$D_N^{\rm np}$	0.9169	0.8392	0.7731	0.7163
e^+e^- $\sigma_N^B = \sigma_N^b K_N$	0.7027	0.5251	0.4066	0.3225
e^+e^- HW σ_N^B	0.7113	0.5354	0.4181	0.3353
e^+e^- PY σ_N^B	0.7162	0.5412	0.4237	0.3400
H-dec.(120) NLL Γ_N^b	0.7580	0.6166	0.5197	0.4477
H-dec.(120) $\Gamma_N^B = \Gamma_N^b D_N^{\rm np}$	0.6950	0.5175	0.4018	0.3207
H-dec.(120) $\Gamma_N^B = \Gamma_N^b K_N$	0.6829	0.5030	0.3858	0.3036
H-dec.(120) HW c. Γ_N^B	0.6842	0.5036	0.3877	0.3076
H-dec.(120) HW no c. Γ_N^B	0.6961	0.5177	0.4011	0.3197
H-dec.(120) PY Γ_N^B	0.6876	0.5080	0.3913	0.3099
H-dec.(500) NLL Γ_N^b	0.6858	0.5265	0.4255	0.3545
H-dec.(500) $\Gamma_N^B = \Gamma_N^b D_N^{\rm np}$	0.6288	0.4418	0.3290	0.2539
H-dec.(500) $\Gamma_N^B = \Gamma_N^b K_N$	0.6178	0.4295	0.3158	0.2404
H-dec.(500) HW c. Γ_N^B	0.6184	0.4279	0.3146	0.2406
H-dec.(500) HW no c. Γ_N^B	0.6286	0.4389	0.3245	0.2491
H-dec.(500) PY Γ_N^B	0.6044	0.4152	0.3036	0.2307
t-dec. NLL Γ_N^b	0.7883	0.6615	0.5735	0.5071
t-dec. NLL $\Gamma_N^B = \Gamma_N^b D_N^{\rm np}$	0.7228	0.5551	0.4434	0.3632
t-dec. $\Gamma_N^B = \Gamma_N^b K_N$	0.7102	0.5397	0.4257	0.3439
t-dec. HW Γ_N^B	0.7325	0.5703	0.4606	0.3814
t-dec. PY Γ_N^B	0.7225	0.5588	0.4486	0.3688

latter used in conjunction with the NLL-resummed calculation, to e^+e^- data on the B-hadron energy fraction x_B, from ALEPH, OPAL and SLD. We found that the Kartvel-

ishvili and the PYTHIA string model are able to fit the data quite well, while the HERWIG cluster model is only marginally consistent. The tuning of the Monte Carlo programs turned out to be essential, since the default parametrizations fare rather badly against the measured x_B spectrum.

Relying on the process-independence of the hadronization, we have predicted the x_B spectrum in Higgs and top decays, using the tuned models, and found results which reflect the quality of the fit to the e^+e^- data. PYTHIA and resummed calculations give consistent results, while the HERWIG predictions are broader and compatible only in some x_B ranges. The effect of matrix-element corrections to $H \to b\bar{b}$ is reasonable, since more events are generated via the exact amplitude at small x_B, which corresponds, at parton level, to hard and large-angle gluon radiation. Comparing the spectra of B hadrons in Z, H and top decays has given similar results to the ones already found in the framework of perturbative fragmentation functions: the B's from top quarks are the hardest, the ones from H are the softest, and the ones from Z lie within the two.

Finally, we have considered data on the moments of the B cross section measured at LEP by the DELPHI collaboration. We have extracted the moments of the non-perturbative fragmentation function, and compared the N-space cross sections given by the NLL computation to those yielded by HERWIG and PYTHIA. We found that tuned HERWIG and PYTHIA are able to reproduce the DELPHI moments, within the quoted error range, even though HERWIG had problems with fitting the e^+e^- x_B data. The N-space predictions in top decay reflect the behaviour of the x_B-space results: PYTHIA is closer to the NLL calculation, and HERWIG yields larger moments. In $H \to b\bar{b}$, all given moments are pretty similar for $m_H = 120$ GeV, while, for $m_H = 500$ GeV, HERWIG is closer to the NLL prediction and PYTHIA yields smaller results. Matrix-element corrections to HERWIG simulations of $H \to b\bar{b}$ decrease the moment values, which is due to the smaller fraction of events at large x_B. We have also pointed out that the moments based on an NLL x_B-space fit, making use of the Kartvelishvili fragmentation model in a range which discards very large and very small values of x_B, are different from the ones obtained after fitting the moments experimentally measured by DELPHI directly.

In conclusion, we believe that our studies and tunings can be a useful starting point to address b-quark fragmentation at the Tevatron and LHC, especially for the analyses of top-quark properties, such as its mass, and for the Higgs studies in the $H \to b\bar{b}$ channel. It will also be interesting to use the parametrizations which we have proposed to study other hadron-level observables not necessarily related to b-quark fragmentation. Moreover, while we deliberately did not aim at fitting any perturbative parameter entering in the Monte Carlo simulation or in the resummed calculation, it will be nonetheless cumbersome comparing parton-level observables and investigating whether further tuning may improve the comparison with the e^+e^- data and affect the hadron-level predictions.

Acknowledgements

We are grateful to M. Cacciari who provided us with the computer code to perform inverse Mellin transforms and fit the Kartvelishvili model to e^+e^- data. We acknowledge M.H. Seymour and T. Sjöstrand for discussions on HERWIG and PYTHIA event generators. Work supported in part by the European Community's Human Potential Programme under contract HPRN-CT-2002-00326, [V.D.].

References

[1] SLD Collaboration, K. Abe et al., Phys. Rev. Lett. 84 (2000) 4300.

[2] ALEPH Collaboration, A. Heister et al., Phys. Lett. B512 (2001) 30.

[3] OPAL Collaboration, G. Abbiendi et al., Eur. Phys. J. C29 (2003) 463.

[4] The Tevatron Electroweak Working Group Collaboration, hep-ex/0507006.

[5] A. Kharchilava, Phys. Lett. B476 (2000) 73.

[6] M. Carena et al., FERMILAB PUB 349 (2000) 185, hep-ph/0010338.

[7] V. Drollinger, Th. Müller and D. Denegri, CERN CMS NOTE 006 (2002), hep-ph/0201249.

[8] E. Richter-Was and M. Sapinski, Acta Phys. Polon. B30 (1999) 1001-1040; V. Drollinger, Th. Müller and D. Denegri, CERN CMS NOTE 054 (2001), hep-ph/0111312.

[9] ATLAS Collaboration, CERN LHCC 15 (1999) 754.

[10] B. Mele and P. Nason, Nucl. Phys. B 361 (1991) 626.

[11] G. Altarelli and G. Parisi, Nucl. Phys. B126 (1977) 298.

[12] L.N. Lipatov, Sov. J. Nucl. Phys. 20 (1975) 95; V.N. Gribov and L.N. Lipatov, Sov. J. Nucl. Phys. 15 (1972) 438; Yu.L. Dokshitzer, Sov. Phys. 46 (1977) 641.

[13] M. Cacciari and S. Catani, Nucl. Phys. B617 (2001) 253.

[14] G. Sterman, Nucl. Phys. B281 (1987) 310.

[15] S. Catani and L. Trentadue, Nucl. Phys. B327 (1989) 323.

[16] G. Corcella and A.D. Mitov, Nucl. Phys. B623 (2002) 247.

[17] M. Cacciari, G. Corcella and A.D. Mitov, JHEP 0212 (2002) 015.

[18] G. Corcella, Nucl. Phys. B 705 (2005) 363 [Erratum-ibid. B 715 (2005) 609].

[19] G. Corcella, I.G. Knowles, G. Marchesini, S. Moretti, K. Odagiri, P. Richardson, M.H. Seymour, B.R. Webber, JHEP 0101 (2001) 010.

[20] T. Sjöstrand, L. Lönnblad and S. Mrenna, hep-ph/0108264.

[21] T. Sjöstrand, L. Lönnblad, S. Mrenna and P.Z. Skands, hep-ph/0308153.

[22] M.H. Seymour, Comput. Phys. Commun. 90 (1995) 95.

[23] G. Miu and T. Sjöstrand, Phys. Lett. B449 (1999) 313.

[24] V.G. Kartvelishvili, A.K. Likehoded and V.A. Petrov, Phys. Lett. B78 (1978) 615.

[25] C. Peterson, D. Schlatter, I. Schmitt and P.M. Zerwas, Phys. Rev. D27 (1983) 105.

[26] M. Cacciari and P. Nason, Phys. Rev. Lett. 89 (2002) 122003.

[27] B.R. Webber, Nucl. Phys. B238 (1984) 492.

[28] B. Andersson, G. Gustafson, G. Ingelman, T. Sjöstrand, Phys. Rept. 97 (1983) 31.

[29] K. Melnikov and A.D. Mitov, Phys. Rev. D70 (2004) 034027.

[30] A.D. Mitov, Phys. Rev. D70 (2004) 034027.

[31] G. Marchesini and B.R. Webber, Nucl. Phys. B238 (1984) 1; ibid. B310 (1988) 461.

[32] T. Sjöstrand and P.Z. Skands, Eur. Phys. J. C39 (2005) 129.

[33] G. Corcella et al., hep-ph/0210213. Version 6.506 available from: http://hepwww.rl.ac.uk/theory/seymour/herwig/herwig65.html

[34] S. Catani, G. Marchesini and B.R. Webber, Nucl. Phys. B349 (1991) 635.

[35] S. Frixione and B.R. Webber, JHEP 0206 (2002) 029.

[36] Yu.L. Dokshitzer, V.A. Khoze and L.H. Orr, Nucl. Phys. B403 (1993) 65.

[37] E. Norrbin and T. Sjostrand, Nucl. Phys. B603 (2001) 297.

[38] M.H. Seymour, Z. Phys. C56 (1992) 161.

[39] M.H. Seymour, *Proceedings of 27th ICHEP, Glasgow, 1994*, LU-TP-94-12.

[40] G. Corcella and M.H. Seymour, Phys. Lett. B442 (1998) 417.

[41] G. Corcella and M.H. Seymour, Nucl. Phys. B565 (2000) 227.

[42] G. Corcella and S. Moretti, Phys. Lett. B590 (2004) 249.

[43] R. Hemingway, OPAL Technical Note TN652.

[44] S. Gieseke, A. Ribon, M.H. Seymour, P. Stephens and B.R. Webber, JHEP 0402 (2004) 005.

[45] S. Gieseke, P. Stephens and B.R. Webber, JHEP 0312 (2003) 045.

[46] M.G. Bowler, Z. Phys. C11 (1981) 169.

[47] P. Skands, http://home.fnal.gov∼skands/stuff/main75.f

[48] DELPHI Collaboration, G. Barker et al., DELPHI 2002-069, CONF 603.

[49] M. Cacciari and E. Gardi, Nucl. Phys. B664 (299) 2003.

[50] M. Cacciari, S. Frixione, M.L. Mangano, P. Nason and G. Ridolfi, JHEP 0407 (2004) 033.